

Title: A human-specific microRNA controls the timing of excitatory synaptogenesis.

Authors: Michael Soutschek¹, Alessandra Lo Bianco¹, Simon Galkin¹, Tatjana Wüst^{1,4}, David Colameo¹, Tomas Germade^{1,5}, Fridolin Gross^{1,6}, Lukas von Ziegler², Johannes Bohacek², Pierre-Luc Germain^{1,2,3}, Jochen Winterer¹, Tatjana Kleele⁷ and Gerhard Schratt^{1*}

Affiliations:

¹ Laboratory of Systems Neuroscience, Institute for Neuroscience, Department of Health Science and Technology, ETH Zürich, Switzerland

² Laboratory of Molecular and Behavioural Neuroscience, Institute for Neuroscience, Department of Health Science and Technology, ETH Zürich, Switzerland

³ Lab of Statistical Bioinformatics, IMLS, University of Zürich, Switzerland

⁴ present address: Ncardia Services B.V., Leiden, The Netherlands

⁵ present address: Laboratory of Epigenetics and Neuroendocrinology, Institute for Neuroscience, Department of Health Science and Technology, ETH Zürich, Switzerland

⁶ present address: CNRS UMR5164 ImmunoConcEpT, University of Bordeaux, France

⁷ Department of Biology, Institute of Biochemistry, ETH Zurich, Zurich, Switzerland..

*Corresponding author: gerhard.schratt@hest.ethz.ch

Keywords: non-coding RNA, microRNA, human synaptogenesis, developmental timing, mitochondria, mitophagy, Pink1

Running title: miR-1229-3p in human excitatory synaptogenesis

Abstract: Neural circuit development in the human cortex is considerably prolonged in comparison to non-human primates, a trait that contributes to the remarkable cognitive capacity of modern humans. Here, we explore the regulatory role of non-coding RNAs, which dramatically expanded during brain evolution, in synapse development of human-induced pluripotent stem-cell derived neurons. Inhibition of a human-specific microRNA, miR-1229-3p, results in accelerated formation of excitatory synapses and enhanced synaptic transmission. Mechanistically, miR-1229-3p controls mitochondrial homeostasis by targeting important regulators of mitochondrial autophagy and fission, such as Pink1. Stimulation of mitochondrial metabolism rescues decreased calcium buffering in miR-1229-3p depleted neurons. Our findings reveal an important function of human-specific miR-1229-3p in developmental timing of human synaptogenesis and generally implicate non-coding RNAs in the control of human connectivity and cognition.

One-Sentence Summary: A human-specific microRNA slows down the formation and maturation of neuronal synapses by reducing mitochondrial metabolism and renewal.

Main Text:

Introduction

The human brain enables remarkable cognitive achievements that are unparalleled in any other species. It contains more neurons and shows an increased size in comparison to the brains of other primates, particularly in the cerebellum and cortex (1). However, this expansion represents an expected scaling across hominids (2) which does not correlate with cognition (3), suggesting that different mechanisms account for human-specific cognitive abilities. In this regard, human neurons lag in development when compared to the developmental timing of other species (a concept called human neoteny), illustrated by a slower reach of the maximal synapse density followed by a delayed pruning of the acquired synapses (1). The resulting prolonged synaptogenesis and synaptic plasticity period has been suggested to be key in the enhanced social and cultural learning of humans (4).

Little is known regarding the genetic mechanisms underlying human-specific aspects of synaptogenesis and plasticity. For example, human-specific non-synonymous base pair substitutions in the *Foxp2* gene, which is mutated in a monogenic speech disorder, lead to increased neurite outgrowth and synaptic plasticity of corticostriatal circuits along with behavioral phenotypes in mice (5). Moreover, expression of the human-specific *Srgap2c* in mice, which originates from a gene duplication, delays synapse maturation in cortical pyramidal neurons (1, 6, 7). However, due to the generally high conservation of protein-coding genes, it has been suggested early on that most phenotypic differences between humans and other primates might be rather caused by changes in non-coding DNA regulating gene expression (8). Regulatory regions of the genome that evolved particularly fast in humans, such as the human accelerated regions (HAR) and human gained enhancers (HGE), represent interesting candidates in this regard (9). In addition to fulfilling gene regulatory functions *in cis*, non-coding DNA is pervasively transcribed into a plethora of non-coding RNA (ncRNA) families that control gene expression *in trans*, such as long non-coding RNAs (lncRNAs) and microRNAs (miRNAs) (10). An expansion in the repertoire of miRNAs was suggested to contribute to the increased complexity of the brain throughout evolution (11, 12). Human miRNA expression in the brain has been profiled previously in adulthood and development from post-mortem tissue samples (13-16). Moreover, the human-specific miR-941 has been investigated with regards to its expression levels in the brain and putative functionality in cell lines (17). However, despite their well-documented role in neuronal development in vertebrates (18), it is unknown whether miRNAs control aspects of human neoteny, such as delayed neuronal maturation and synaptogenesis.

Results

A glia-free cell neuronal cell culture model to study human excitatory synaptogenesis.

To systematically profile human miRNA expression over the course of synaptogenesis, we established glial-free 2D cultures of human induced-pluripotent stem cell (hiPSC) derived excitatory cortical neurons by modifying a previously published Ngn2-overexpression protocol (19) (Fig. 1a; Suppl. fig. S1a-b; materials and methods). miRNAs are highly conserved between different cell types and across species. The omission of glial cells was therefore a prerequisite for faithful detection of miRNAs exclusively in excitatory cortical neurons. Based on immunostaining for excitatory synaptic marker proteins PSD95 and SYN1, neurons cultured with our protocol (hereafter referred to as induced glial-free neurons, or igNeurons for short) begin to form structural synapses (synaptic co-clusters) at 15 days of differentiation (Fig. 1b). We further observed spine-like structures, a hallmark of excitatory synapse maturation, from day 27 on (Suppl. fig. S1c). When quantifying three independent igNeurons differentiations, we observed that PSD95-Synapsin co-cluster density steadily increases until day 27, before reaching a plateau (Fig. 1c, Suppl. fig. S2). On the other hand, dendritic complexity expands over the entire time course, with the steepest rise after day 27 (Suppl. fig. S3). Calcium (Ca-) imaging upon transduction with the calcium indicator GCaMP6f shows spontaneous activity of igNeurons from day 21 on (Fig. 1d-e). Activity can be blocked by the AMPAR antagonist NBQX, suggesting that calcium signals are generated by synaptic activity (Suppl. Fig. S4b-c). Patch-clamp recordings further showed that igNeurons could generate multiple action potentials upon depolarizing current injections, confirming their ability to maintain repetitive firing (Suppl. fig. S4d). Taken together, human igNeurons form functional excitatory synapses within 3-4 weeks, which is comparable to previous protocols using Ngn2-induced neurons in the presence of mouse astrocytes (19). Molecular characterization of igNeurons using ribosomal depletion RNA-seq and label-free proteomics showed widespread gene expression changes until day 27, consistent with prevailing morphological changes, such as the formation of excitatory synapses, in this time window (Fig. 1f; Suppl. fig. S5-7). For example, expression of genes encoding for excitatory synaptic proteins (SYN1, GRIA2/4, GRIN2A/B) follow the pattern of our synaptic co-cluster and calcium imaging quantification (Suppl. fig. 6e). Plotting the scaled expression of synapse-associated genes (Suppl. fig. S6f-g), together with the corresponding proteins and the values obtained from the synapse co-cluster analysis (cf. Fig. 1c), shows that all three measurements follow a similar pattern (Fig. 1g), whereby RNA expression precedes the morphological development by roughly one time point or six days (Fig. 1g). Thus, developmental gene expression profiles in igNeurons should be useful to predict potential functional regulators of excitatory synaptogenesis.

Figure 1)

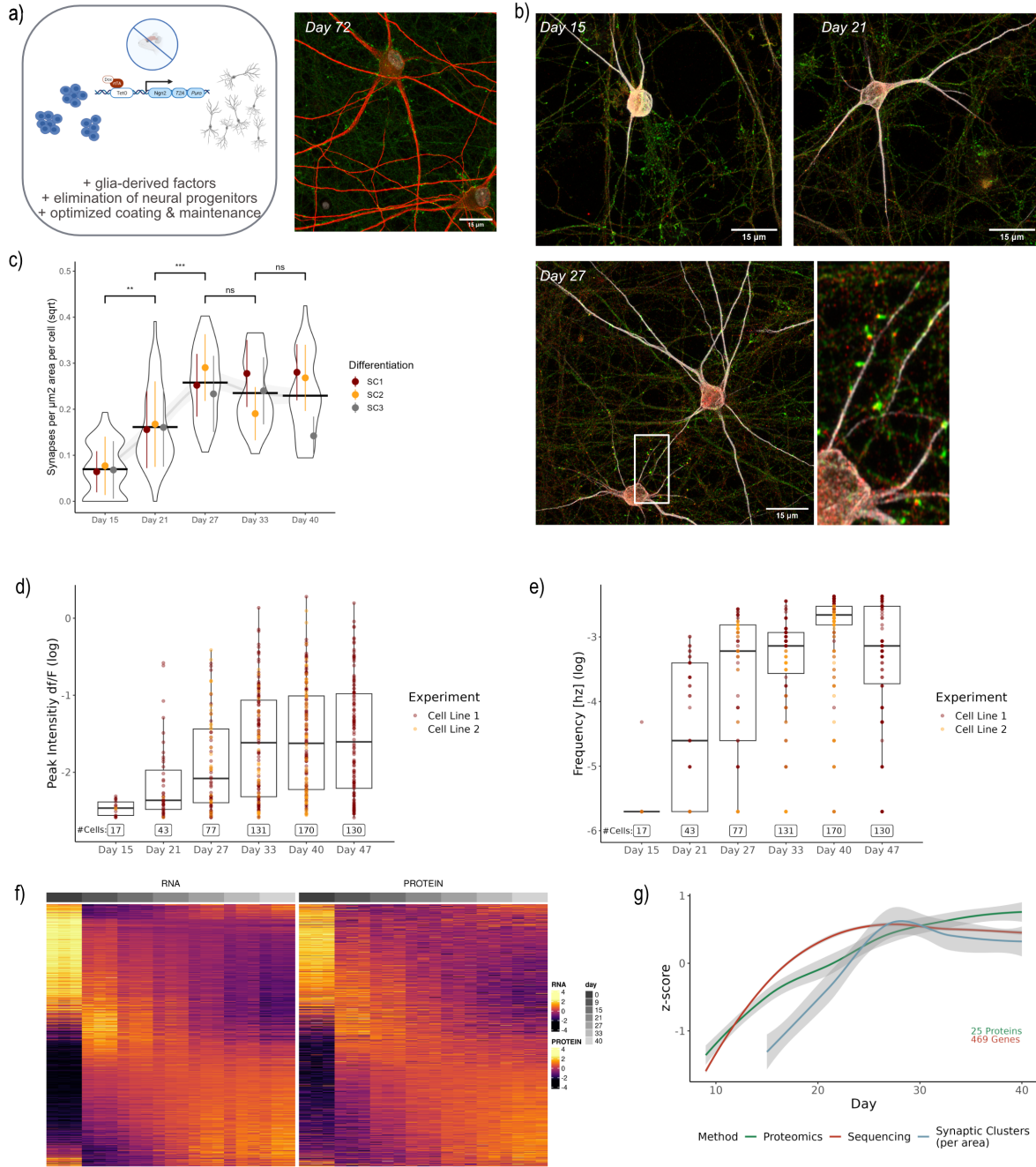


Fig. 1. A glial-free protocol to study human excitatory synapse development

a) Overview of our protocol to differentiate human neurons without the requirement to add glial cells together with an example of igNeurons cultured for over 10 weeks and stained for MAP2 (red) and SYN1 (green). b) Example images of igNeurons used for the quantification of synapse development at three different time points. Shown is MAP2 in grays, SYN1 in green and PSD95 in red. c) Synapse co-cluster quantification over five time points from three differentiations (236 pictures in total, two coverslips (CVS) were imaged per time point and differentiation). The detected number of co-clusters is normalized by the number of neurons and dendritic area in each image. Shown are violin plots of all datapoints together with the mean and standard deviation of each differentiation. Statistical analysis was performed on square root transformed values. A robust linear model was applied over the aggregated means of each day and differentiation to account for outliers in any of the time points (~ day + differentiation).

Statistical comparisons between time points were acquired by applying post-hoc analysis with emmeans. Shown are only statistical comparisons between neighboring time points. (** = p-value < 0.01, *** = p-value < 0.001) d-e) Quantification of the normalized Ca-imaging amplitude (df/F) and frequency (log) over the time course of neuronal differentiation. Measured were two different cell lines. On average, calcium spike activity of igNeurons is higher compared to previous protocols using Ngn2-induced neurons in the presence of mouse astrocytes (20). f) Heatmap indicating scaled expression values of mRNAs and corresponding proteins. Each line depicts one gene, each column one replicate. Plotted are the top 1000 significantly changing genes (FDR < 0.01) and the corresponding proteins during the neuronal time points. In total, 11'799 genes (FDR < 0.01 & logFC > 2) and 2'839 proteins (FDR < 0.01) changed significantly over the full time course according to the ribosomal depletion sequencing and label-free proteomics. The igNeurons time course data can be further accessed at <https://ethz-ins.org/igNeuronsTimeCourse>. g) Smoothed means of scaled RNA expression levels of synapse-associated genes (Cluster 9, see Suppl. fig. S6f-g), the corresponding protein expression levels and log-scaled smoothed means of the synaptic co-cluster analysis.

The ncRNAome during human excitatory synaptogenesis

Of note, mRNA and protein expression trajectories are uncorrelated for a group of genes (Suppl. fig. S7d-e), suggesting the involvement of post-transcriptional regulatory molecules, such as ncRNAs, in human excitatory synaptogenesis. In agreement with this, we observed extensive developmental gene expression changes of regulatory long non-coding RNAs, such as lncRNAs and circRNAs (Suppl. fig. S8-9), in our Ribo-minus RNA-seq dataset. However, for this initial study, we decided to focus on miRNAs due to their well-established role in synapse development in other vertebrates. Therefore, we performed small RNA sequencing on the same differentiations that were processed for previous analyses (cf. Fig. 1, Suppl. fig. 10a). We identified 339 significantly changing miRNAs over the entire time course, of which 181 were significantly changing when considering only neuronal days (day 9 – day 40, FDR < 0.05) (Fig. 2a). In addition, we also quantified snoRNAs (with 81 significantly changing, FDR < 0.05) and piRNAs (122 significantly changing, FDR < 0.05) (Suppl. fig. S10c). Clustering the miRNA expression dataset according to similar expression trajectories rendered a total of 6 independent clusters (Suppl. fig. S11a). Many miRNAs which are known to be involved in neuronal morphogenesis based on rodent studies (e.g., miR-181, miR-124, miR-134) are found in cluster 2 (“begin up”; Suppl. fig. S11b), which features miRNAs that are rapidly induced after the stem cell-neuron transition (day 9 onwards). In contrast, miRNAs known to be involved in synaptic plasticity (e.g., miR-129) (18) are present in cluster 4 (“late up”; Suppl. fig. S11c) which is characterized by a later induction (day 27 onwards).

We next attempted to characterize human-specific features of miRNA regulation in more detail. Towards this aim, we first correlated our miRNA expression data to a smallRNA sequencing dataset obtained from induced mouse neurons (see methods). Thereby, we found that out of the 233 miRNAs commonly detected in both datasets, 181 change significantly during human neuronal differentiation (FDR < 0.05, all time points). Expression patterns of these 181 miRNAs were mostly correlated between human and mouse (Suppl. fig. S11d-e), except for 15 miRNAs which showed strongly anti-correlated expression dynamics, as exemplified by miR-708 (Fig. 2b, Suppl. fig. S11f). We further searched for miRNAs whose sequences are not conserved in other species, including non-human primates. Employing the conservative approach of searching for orthologs in other species by reciprocal blasting of all listed human miRNA precursors of miRbase version 22 (see methods), we found that only a small fraction

of miRNAs can be safely classified as human-specific (25 miRNAs with no more than 60% sequence conservation in any of the tested species) (Suppl. Table 1-5) in agreement with previous publications (17, 21). Additionally, we discovered 52 miRNAs with human-specific seed changes which are expected to have unique target genes in humans. Among this conservative estimate of a total of 77 “human-specific” miRNAs, only four (the newly evolved miR-4745-5p and miR-941, as well as the seed mutants miR-1229-3p and miR-3141) were expressed in our dataset (Fig. 2c-d). While miR-941 is consistently expressed at high levels, miR-4745-5p and miR-3141 change mostly from stem cell to neuron conversion and stay rather constant during neuronal maturation. miR-1229-3p represents the only human-specific miRNA with a dynamic expression pattern during the neuronal days of differentiation, suggesting a role in human synaptogenesis. This finding was further corroborated when we performed gene-wise linear regression of miRNA expression profiles with the neurodevelopmental trajectory inferred by synapse density quantification (cf. Fig. 1c) from the same neuronal differentiations (Fig. 2e). In contrast to the other three human-specific miRNAs, miR-1229-3p expression closely follows synapse density development, as do known regulators of synaptogenesis such as miR-181c-5p (22, 23).

Based on a structural conservation analysis of all human miRNA precursors with mismatches in orthologs found in primates (excluding marmoset), miR-1229-3p shows the lowest structural conservation index, despite a high sequence similarity (Fig. 2f, Suppl. fig. S12a). This lack of structural conservation is further illustrated when plotting the predicted secondary structures of human and chimp pre-miR-1229 (Fig. 2g). Since the predicted chimp pre-miR-1229 is lacking a 2-nucleotide overhang at the 3’end of the precursor required for efficient Dicer-mediated processing (24), no production of mature miR-1229-3p is expected in chimpanzee. In addition, alignment of hsa-pre-miR-1229 with blasted sequences of higher apes shows the presence of four human-specific point mutations, one of which is located in the seed region (Fig. 2h). In agreement with the non-functionality of a putative chimp-miR-1229, expression of the chimp mir-1229 mirtron, in contrast to its human counterpart, was unable to downregulate a perfect miR-1229-3p binding site reporter in a luciferase assay (Fig. 2i, Suppl Fig. 12b). Finally, to assess the conservation of predicted miR-1229-3p targets, we used scanMiR to inspect 3’UTR sequences that we extracted from the chimp genome by lifting over human coordinates from expressed 3’UTRs for potential miR-1229-3p binding sites (see methods). We noticed that almost all binding sites are very well conserved between human and chimpanzee, even regarding their predicted strength (Suppl. fig. S12c). This pattern holds similarly true for all expressed miRNAs (Suppl. fig. S12d), suggesting that evolutionary adaptation of miRNA regulation primarily occurred on the miRNA rather than on the target side. Taken together, four point-mutations within the miR-1229 gene enabled efficient Dicer-mediated processing and the recognition of evolutionary conserved target genes in human neurons.

Figure 2

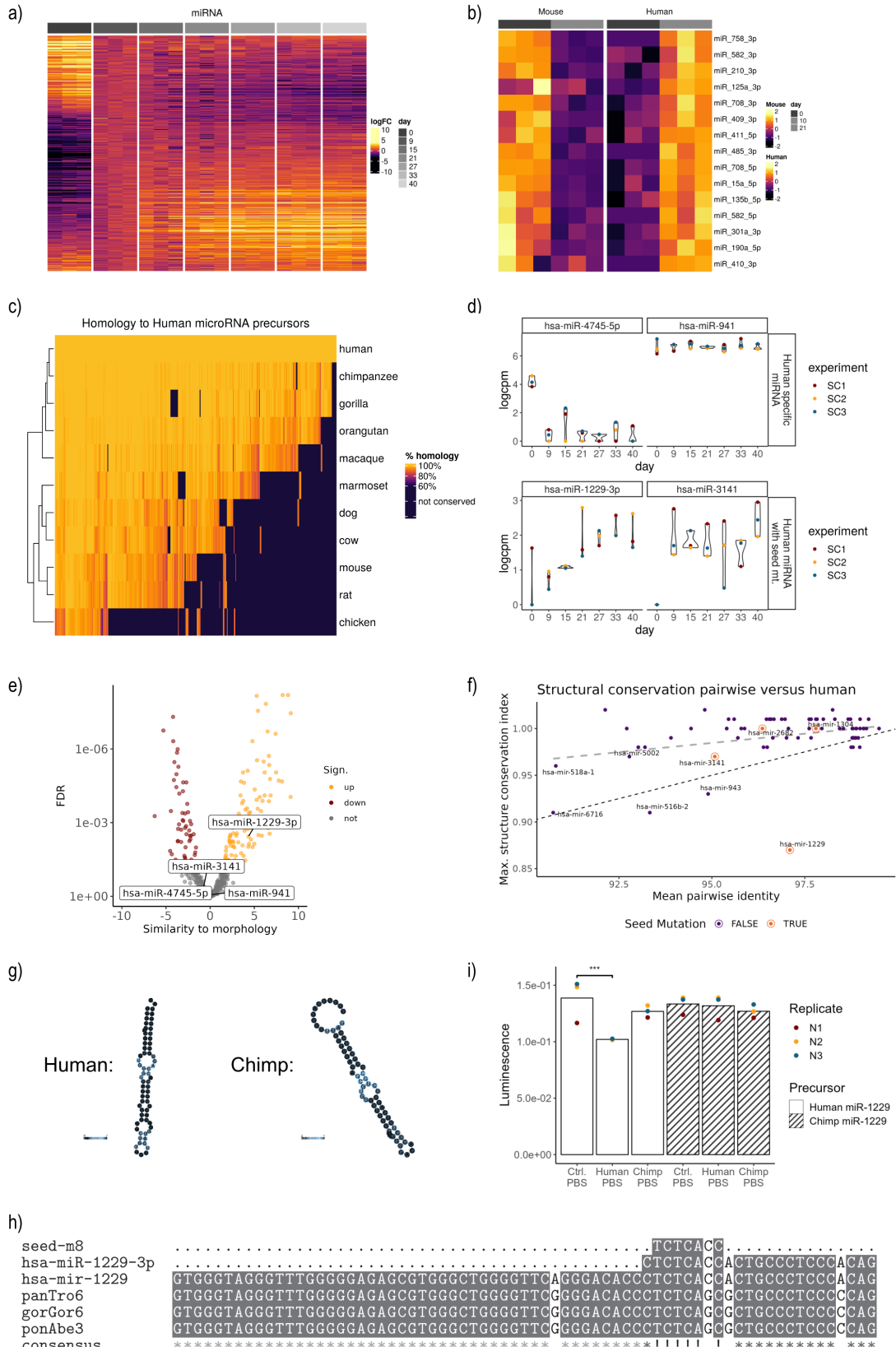


Fig. 2. The ncRNAome during human excitatory synapse development

a) Heatmap of significantly changing miRNAs over the time course of excitatory synapse development (FDR < 0.05, logFC normalized to day 9). b) Heatmap showing the scaled logcpm values of conserved miRNAs between mouse and human that differ in their expression

dynamics. Shown are days 0 and 10 (mouse) and days 0 and 21 (human) (see Suppl. fig S11e for the full time course). c) Heatmap showing the percent homology of expressed human miRNA precursors with orthologs identified by reciprocal blast in selected species. Sequences with less than 60% homology were considered non-homologous. d) Expression examples for human-specific miRNAs not found in other genomes (upper row) and miRNAs with a human-specific seed mutation (lower row) during human neuronal differentiation. e) Volcano plot showing the significance and strength of a regression of each miRNA's expression on excitatory synaptic co-cluster formation across days. f) Pairwise structural conservation analysis of expressed human miRNA precursors with at least one mismatch identified in analyzed species across primates (excluding marmoset). Plotted is the mean identity of the contrasted precursor sequences on the x-axis and the structural conservation index generated by RNAz on the y-axis (following an idea of McCreight et al (25), see methods). The grey dashed line indicates the linear regression of all analyzed precursors. The black reference line (slope = 0.01 and intercept = 0) roughly marks a threshold below which miRNA precursors can be regarded as not structurally conserved. g) RNAfold secondary structure prediction of human pre-miR-1229 and the putative ortholog found in chimpanzees. h) Sequence alignments of hsa-miR-1229-3p, its seed sequence and precursors as well as orthologs among hominids (panTro6 = chimpanzee, panGor6 = gorilla, panAbe3 = orangutan). i) Luciferase measurements of miR-1229 overexpression constructs transfected together with miRNA perfect binding site reporters in HEK cells ($N = 3$, statistics: linear model (~ condition + replicate), post-hoc analysis with emmeans, *** = p-value < 0.001).

Human-specific miR-1229-3p regulates the timing of excitatory synaptogenesis.

Using microRNA qPCR and single-molecule fluorescent in-situ hybridization (FISH), we confirmed that miR-1229-3p is dynamically expressed over the course of human neuron differentiation, in a similar way as miR-181c, a known regulator of neuronal morphogenesis in rodents (Fig. 3a-b). Together with the unique evolutionary features described above, this led us to consider the possibility that miR-1229-3p might be involved in the regulation of excitatory synapse development of human neurons. To interfere with miR-1229-3p expression, we delivered locked nucleic acid (LNA) modified antisense oligonucleotides directed against miR-1229-3p (pLNA-1229) to igNeurons via bath application in the culture media. In addition, we included pLNAs directed against miR-181c-3p (pLNA-181) or a corresponding scrambled control sequence (pLNA-Ctrl) in our experiments. Using a fluorescently labelled pLNA-Ctrl, we confirmed that pLNAs are taken up at nearly 100% efficiency, remain stable inside the cells and don't cause detrimental effects on the neuron morphology even at high concentrations (Suppl. fig. S13). miRNA qPCR further confirmed that the pLNAs specifically decrease the expression of the cognate miRNA (Fig. 3c).

To test the functional role of miR-1229-3p over the course of excitatory synapse development, we applied pLNAs from day 9 on and monitored synaptic co-cluster density and dendritogenesis. We focused on two time points, one during the linear synaptic growth phase (day 21) and one during the plateau phase (day 33) (Fig. 3d).

Remarkably, synapse co-cluster density analysis revealed a significant increase of synaptic co-clusters at day 21 upon depletion of miR-1229-3p compared to the pLNA-Ctrl and pLNA-181 conditions. This effect was no longer seen at day 33 (Fig. 3e, Suppl. fig. S14a). Examining PSD95 and SYN1 density individually showed that increased synapse density in pLNA-1229 treated neurons is mostly driven by enhanced presynaptic differentiation (Suppl. fig. S14b-e). Inhibition of miR-181c-5p showed a trend towards more synapses at the plateau phase (day 33),

which however did not reach statistical significance. Surprisingly, quantification of dendritogenesis showed a decrease of dendritic complexity upon depletion of miR-1229-3p specifically at the later time point (Fig. 3f; Suppl. fig. S15a-c). Together, these results suggest that miR-1229-3p initially functions as a repressor of excitatory synapse formation but is required for dendritic branching during later stages of human neuron development.

To characterize the functional properties of igNeurons depleted from miR-1229-3p, we performed patch-clamp recordings of spontaneous excitatory postsynaptic currents (sEPSC) during the plateau phase when synapses had sufficiently matured (day 40-42) (Fig. 3g-h). At this time point, igNeurons displayed spontaneous activity – a proxy for functional synapses and cell-cell communication – at a similar frequency as human Ngn2-neurons cultured together with astrocytes for 30-35 days (26), further confirming the suitability of our protocol to investigate human excitatory synapse development. Interestingly, sEPSC quantification revealed a significantly higher charge transfer in miR-1229-3p depleted neurons in comparison to the control condition (Fig. 3i). Neurons treated with the pLNA-1229 showed in addition a trend towards a higher sEPSC amplitude ($p = 0.051$), while the sEPSC frequency as well as rise and decay time were not changed (Fig. 3i, Suppl. fig. S16a-c). Besides sEPSC-events, we also detected occasional large-amplitude bursts (Fig. 3h, inset). Focusing on these bursts, we again observed a significant increase in the total charge transfer upon depletion of miR-1229-3p, as well as a trend towards an increased burst peak amplitude ($p = 0.05$) (Fig. 3j). The burst duration remained unchanged (Suppl. fig. S16d). Together, these results demonstrate that the human-specific miR-1229-3p controls the developmental timing of excitatory synaptogenesis and impacts excitatory synaptic function.

Figure 3

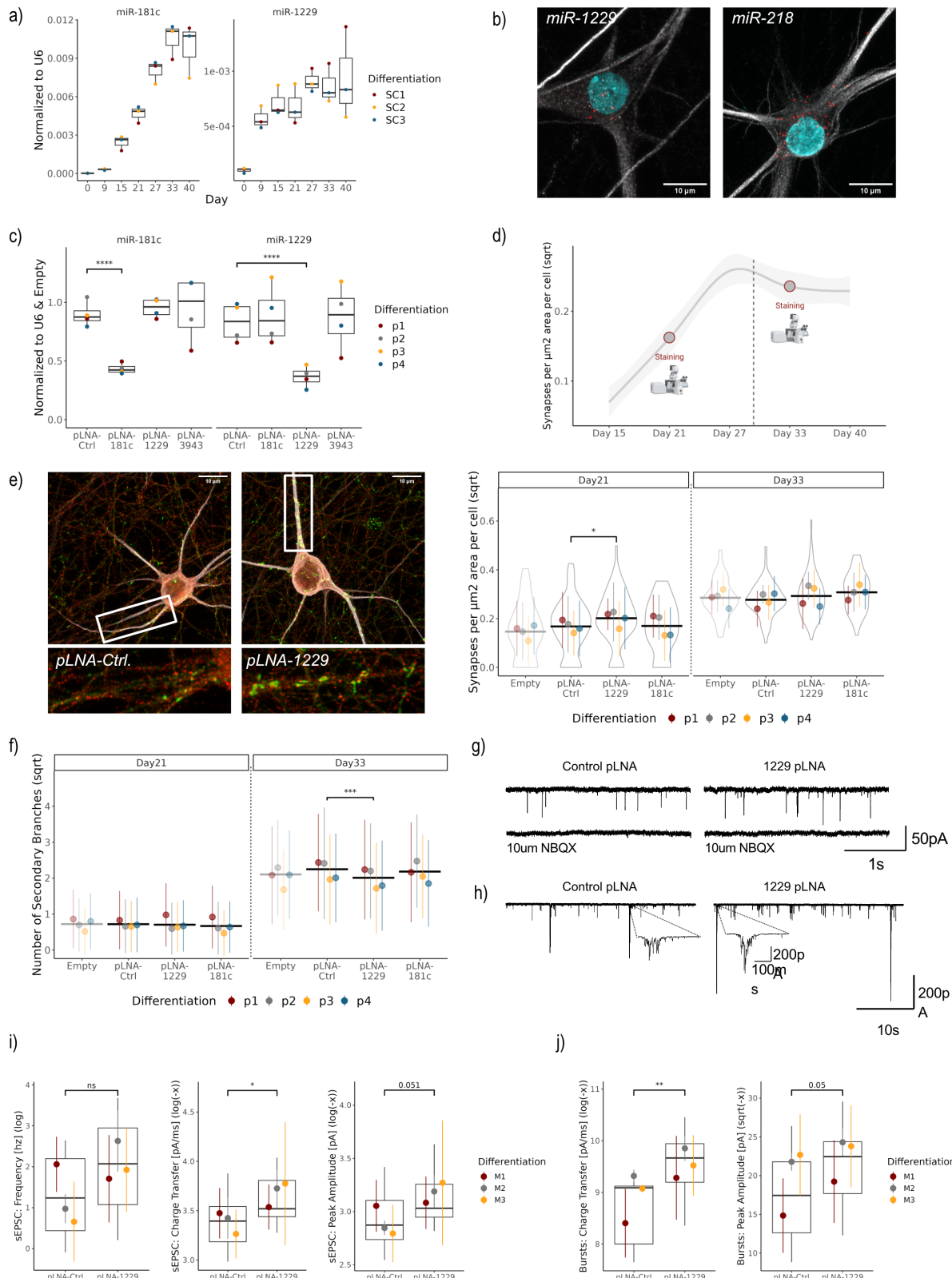


Fig. 3. Human-specific miR-1229-3p restricts excitatory synapse development.

a) TaqMan miRNA qPCRs for miR-1229-3p and miR-181c-5p on the time course samples used for the small RNA sequencing (Fig 2e, g). b) Single-molecule miRNA FISH showing cytoplasmic localization of miR-1229-3p and miR-218-5p in igNeurons (Day 40). miRNA FISH signal in red, MAP2 in gray and Hoechst in cyan. c) TaqMan qPCR for indicated miRNAs

using RNA from igNeurons (day 21) following pLNA application (day 9). The primate-specific miR-3943 served as further specificity control. Expression levels were normalized to U6 and the “Empty” condition. Statistical analysis was performed on the logarithmic values normalized to U6 ($N = 4$ differentiations, statistics: linear model (\sim condition*target + differentiation*target), post-hoc analysis with emmeans) d) Smoothed mean of all images used for the synapse quantification in Fig. 1c) with circles indicating the two time points (day 21 & day 33) at which morphology was assessed upon pLNA addition. e) Representative images of pLNA-treated igNeurons (pLNA-1229 & pLNA-Ctrl) are displayed on the left (MAP2 in gray, PSD95 in red and SYN1 in green). Quantification of synaptic co-clusters (PSD-95/SYN1) in pLNA-treated igNeurons at day 21 and 33 of four independent differentiations is shown on the right (64 images per condition and time point in total, taken from two CVS each). Shown are violin plots of all datapoints together with the mean and standard deviation of each differentiation. Values were transformed with the square root to account for skewed data. A robust linear model was applied over the aggregated means of each pLNA-condition and differentiation (\sim condition + differentiation). Post-hoc analysis was done using emmeans. f) Quantification of the number of secondary dendrite branches in pLNA treated igNeurons at day 21 and 33 of four independent differentiations (32 tile images per condition and time point in total). Shown are the mean and standard deviation of all datapoints of each differentiation. Statistical analysis was performed on the aggregated means of each pLNA-condition and differentiation with a robust linear model (\sim condition + differentiation). Post-hoc analysis was done using emmeans. g) Spontaneous excitatory postsynaptic current (sEPSC) traces of pLNA-treated igNeurons with or without NBQX. h) Example traces of sEPSC bursts recorded by patch-clamp. i-j) Quantification of sEPSC frequency, charge transfer and amplitude (recorded from 15 (pLNA-Ctrl) and 21 (pLNA-1229) neurons of three independent differentiations) (i) as well as quantification of charge transfer and amplitude in recorded sEPSC bursts (obtained from 11 (pLNA-Ctrl) and 21 (pLNA-1229) neurons of three independent differentiations) (j). Shown are box plots of all datapoints together with the mean and standard deviation of each differentiation. Values were log-transformed and aggregated per cell. A linear model plus emmeans were used for the statistical analyses (\sim condition + differentiation). (* = p-value < 0.05, ** = p-value < 0.01, *** = p-value < 0.001, **** = p-value < 0.0001)

miR-1229-3p regulates genes involved in mitochondrial homeostasis

The observation that miR-1229 depletion leads to pronounced morphological and functional changes during human excitatory synapse development prompted us to further investigate the molecular mechanisms underlying these effects. We therefore profiled the protein-coding transcriptome of pLNA-1229-, pLNA-181c-, pLNA-Ctrl-treated, as well as untreated igNeurons by polyA-RNA-sequencing during the synaptic growth period at day 21 (cf. Fig. 3d, Suppl. fig. S17-18). When comparing the transcriptome of pLNA-1229 to pLNA-Ctrl-treated and untreated neurons (see methods), we detected 414 candidate differentially expressed genes (cDEG) (FDR < 0.5; Fig. 4a). Strikingly, the vast majority of cDEGs were downregulated upon miR-1229-3p inhibition, suggesting that most of the observed changes are not a primary effect due to the loss of miRNA repression, but rather secondary gene expression changes (Fig. 4a, Suppl. fig. S17b). To gain further insight into the cellular pathways regulated by miR-1229-3p, we performed gene ontology (GO-term) analysis of cDEGs (Fig. 4b, Suppl. fig. S17c). Among the top 15 biological processes enriched in the dataset, many were associated with mitochondrial function. While most mitochondrial proteins are transcribed from the nuclear genome, mitochondria still retain their own DNA (mtDNA) encoding for 13 proteins of the

electron transport chain. Strikingly, plotting all protein-coding genes transcribed from mtDNA showed a specific downregulation of almost all of them in the pLNA-1229 condition (Fig. 4c), while various genes related to mitochondrial metabolism are upregulated upon miR-1229-3p knockdown (Suppl. fig. S19a). Since neither the expression of nuclear-encoded mitochondrial complex I genes (Suppl. fig. S19b) nor predicted nuclear targets of the mitochondrial transcription factor TFAM were altered (Suppl. fig. S19c), miR-1229-3p inhibition appears to specifically affect mitochondrial gene expression. This effect is not due to increased mutation frequency in the mitochondrial genome, since the number of SNPs in mitochondrial transcripts is not altered by miR-1229-3p inhibition (Suppl. fig. S19d-e).

Human brains require more energy than those of closely related primates (27), and the speed of neuronal development is chiefly determined by the mitochondrial metabolic rate (28). In agreement, we see that the expression levels of mtDNA encoded genes as well as the abundance of mitochondrial ribosomal proteins are highly dynamic throughout neuronal development (Suppl. fig. S20a-b). We therefore decided to study a potential regulation of mitochondrial function by miR-1229-3p in further detail. To identify direct effectors of miR-1229-3p, which might function upstream of the global changes in the mitochondrial transcriptome, we focused on upregulated genes within the pLNA-1229 dataset (Suppl. fig. S17d). In the GO-term analysis, top enriched biological processes with upregulated genes included “autophagy of mitochondrion” and “membrane fusion” (Fig. 4b). A more refined GO-term analysis specifically on the candidate upregulated genes in the pLNA-1229 dataset ($p\text{-value} < 0.05$), further showed a specific enrichment for terms related to autophagy (Fig. 4d). Four of the autophagy-related upregulated genes contain high-affinity (7mer-a1 or stronger) miR-1229-3p binding sites (Fig. 4e). Among those, PTEN-induced kinase 1 (Pink1) was the most significantly upregulated miR-1229-3p target gene in the pLNA-1229 dataset, containing an 8mer binding site near the polyA signal of its 3'UTR. Pink1 is involved in mitochondrial quality control by guiding Parkin to depolarized mitochondria, thereby triggering a special form of autophagy known as mitophagy (29). Using luciferase assays with a wild-type and miR-1229-3p binding site mutant Pink1 3'UTR reporter gene constructs, we were able to validate Pink1 as a direct target of miR-1229-3p in a human cell line and rat primary neurons (Fig. 4f, Suppl. fig. S20c). In conclusion, our results indicate that miR-1229-3p depletion profoundly impacts mitochondrial gene expression and identify the mitophagy regulator Pink1 as a direct miR-1229-3p target gene.

Figure 4

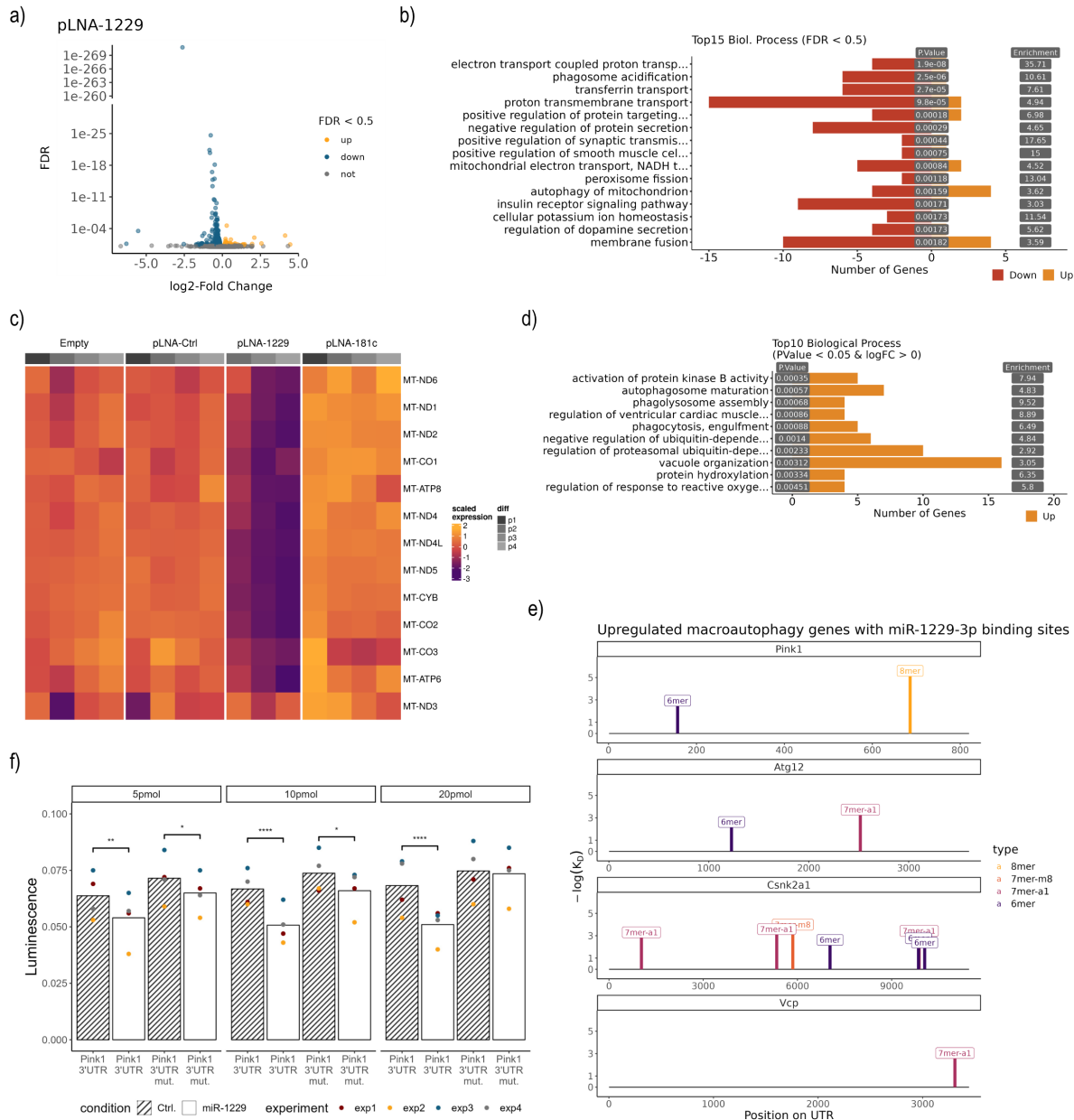


Fig. 4. miR-1229-3p regulates genes involved in mitochondrial homeostasis.

a) Volcano plot indicating significantly changing genes upon miR-1229-3p depletion. Upregulated genes ($FDR < 0.05$) are displayed in yellow, downregulated genes ($FDR < 0.05$) in blue. b) GO-Term analysis (biological processes) of significantly changing genes ($FDR < 0.5$) in the pLNA-1229 condition. Displayed are the top 15 significant GO-Terms with less than 500 genes annotated. The number of significantly changing genes within each GO-term is represented by the red (downregulated) and yellow (upregulated) bars. c) Heatmap showing the scaled expression of genes encoded by the mitochondrial genome in pLNA-treated igNeurons. d) GO-Term analysis (biological processes) of upregulated genes ($p\text{-value} < 0.05$) in pLNA-1229 treated igNeurons. The top 10 most significant GO-terms with more than 15 and less than 500 annotated genes are displayed. Yellow bars indicate the number of genes associated with each GO-Term. e) Predicted miR-1229-3p binding sites in 3'UTRs of genes upregulated in pLNA-1229 treated igNeurons and associated with the GO-Term autophagy. Shown are $\log(K_D)$ values (ScanMiR-predicted miRNA binding site affinity (30)) of canonical binding sites and their position on the 3'UTR. f) Luciferase measurement of Pink1 3'UTR constructs transfected

into HEK-cells together with synthetical miR-1229-3p or control (Ctrl.) mimics (5-20 pmol). “Pink1 3’UTR mut.” contains three point mutations in the 8mer binding site (Fig. 4e). A linear model with an interaction effect for the sequence, miRNA mimic and miRNA mimic amount (including a fixed effect for the experiment) was used for the statistical analysis (~ condition*sequence*amount + experiment). Statistical comparisons were acquired using emmeans by comparing the two conditions separately per amount and sequence (sequence|condition|amount, reference = Ctrl., N = 5). (* = p-value < 0.05, ** = p-value < 0.01, *** = p-value < 0.0001)

miR-1229-3p controls mitochondrial homeostasis during human excitatory synaptogenesis.

Mitochondria homeostasis plays an essential role in regulating synaptic signaling and development (28, 31). Given the profound impact of miR-1229-3p on the expression of mitochondrial genes and the identification of Pink1 as a direct miR-1229-3p target gene, we assessed the effects of miR-1229-3p depletion on mitochondrial morphology and homeostasis. To monitor mitochondrial morphology in human neurons, we performed stainings with the membrane potential sensitive dye Mitotracker (CMXRos) on day 27 of the neuronal differentiation. We noticed the frequent presence of Mitotracker “puncta” with a high local intensity almost exclusively in the soma of neurons treated with pLNA-1229 (Fig. 5a). Such mitochondrial accumulations have been previously associated with mitophagy driven by the Pink1/Parkin pathway (32). Mitotracker “puncta” repeatedly co-localized with the lysosomal marker Lamp2 (Fig. 5b), suggesting that they represent mitophagosomes (33). Moreover, human neurons treated with pLNA-1229 showed a significantly higher somatic entropy and intensity of the Mitotracker signal in comparison to neurons treated with the scrambled control (Fig. 5c-d), indicating elevated mitochondrial fragmentation. Together, these observations suggest that premature excitatory synaptogenesis in miR-1229-3p depleted human neurons correlates with enhanced mitophagy. These findings are consistent with earlier studies from *Drosophila* and *C. elegans*, which reported reduced synaptogenesis in several mutants of the autophagy pathway (34).

In addition to promoting mitophagy, the miR-1229-3p target gene Pink1 has been shown to promote mitochondrial fission (35). In neurons, mitochondrial fission is required for mitochondria to be transported to axons and has been shown to be essential for synapse development (36, 37). We therefore quantified the Mitotracker signal in processes of human neurons at day 23 and found a higher number of axonal mitochondria in the pLNA-1229 condition (Fig. 5e, Suppl. fig. S21a-e). In addition, we performed a detailed analysis of mitochondria ultrastructure using live-cell super resolution imaging of human neurons at day 29 and day 36 (Fig. 5f). Consistent with enhanced mitochondrial fission upon miR-1229-3p inhibition, mitochondrial organelle size (area and length) was significantly reduced in pLNA-1229 compared to pLNA-Ctrl treated igNeurons at day 36 (Fig. 5g, Suppl. fig. S22).

Excessive mitophagy reduces the cellular mitochondrial content, possibly causing reduced mitochondrial metabolism (38, 39). This in turn would shift the provision of energy supply towards glycolysis, reflected by enhanced lactate production (Fig. 5h). In line with a decreased mitochondrial metabolic activity upon sustained miR-1229-3p depletion, we observed a significantly increased lactate concentration in the media collected from pLNA-1229-treated neurons in comparison to control neurons at day 36 (Fig. 5i). Besides energy provision, neuronal mitochondria play an important role in calcium buffering and uptake upon stimulation, particularly at presynaptic termini (31). Accordingly, it has been shown that mitochondria

deactivation or a lack of mitochondria leads to elevated calcium levels in the cytoplasm and at synapses upon stimulation (40, 41). We therefore performed Ca-imaging at day 37 of the neuronal differentiation and indeed observed an increase of the calcium signal amplitude in miR-1229-3p depleted neurons in comparison to the control (Fig. 5j) while the peak duration was not changed (Suppl. fig. S23). These results corroborate the electrophysiological recordings of spontaneous bursts in igNeurons treated with pLNA-1229 (cf. Fig. 3j and Suppl. fig. S16d). Strikingly, activation of mitochondria by the addition of GSK-2837808A and AlbuMAX (28) rescued the elevated calcium signal amplitude (Fig. 5j), demonstrating that impaired calcium buffering in miR-1229-3p depleted human neurons is a consequence of disturbed mitochondrial function. In conclusion, we show that interfering with miR-1229-3p during synaptogenesis enhances mitophagy and mitochondrial fission, which ultimately leads to defects in calcium buffering and metabolic function.

Figure 5

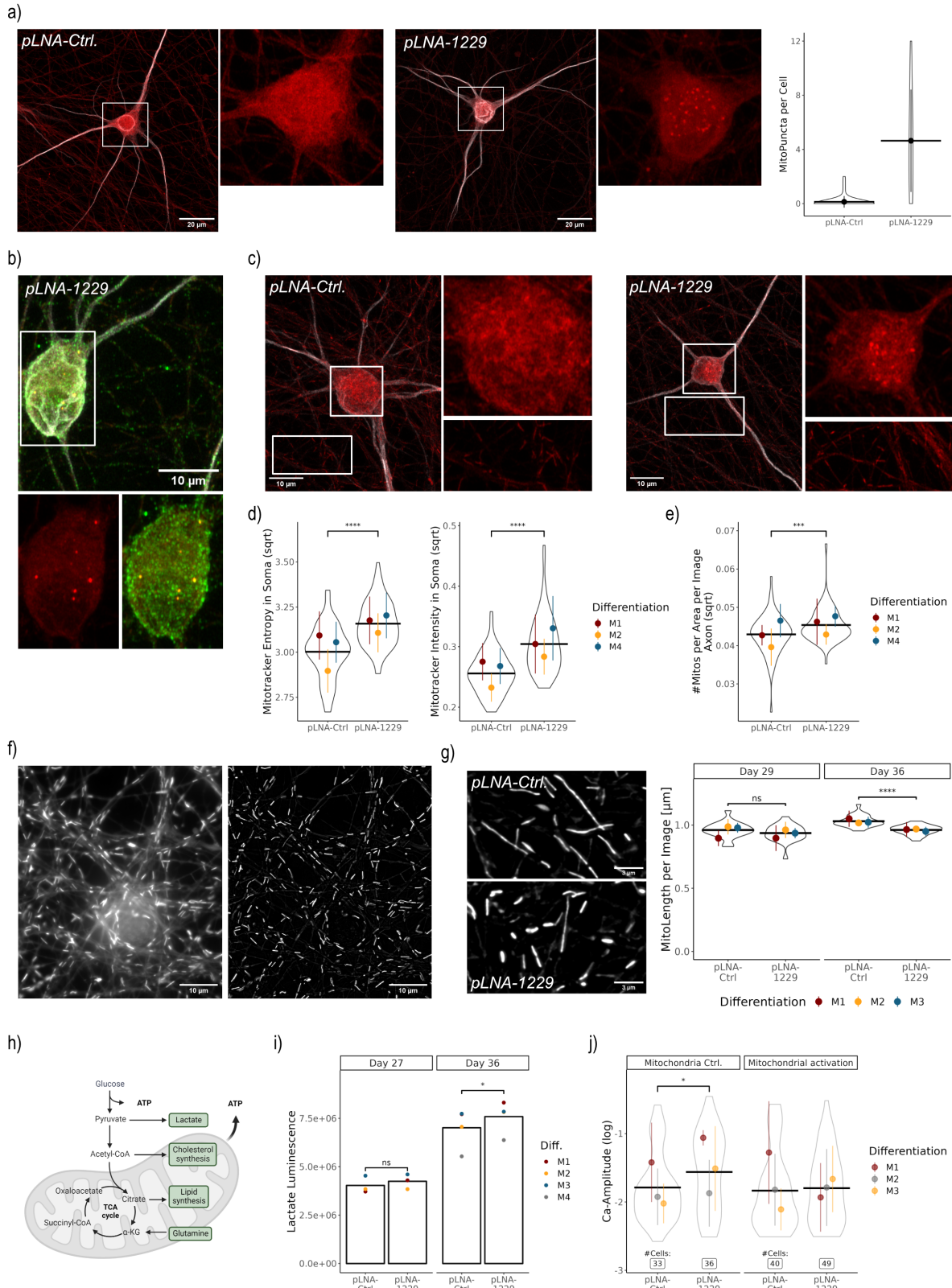


Fig. 5. miR-1229-3p controls mitochondrial homeostasis during human excitatory synapse development a) Confocal images displaying neurons stained for MAP2 (grays) and with Mitotracker CMXRos (1:7500, ca. 130nM, red)) at day 27. Quantification was performed on 38 neurons of the pLNA-Ctrl condition and 39 neurons of the pLNA-1229 condition imaged from two CVS. Shown are violin plots of all datapoints together with the mean and standard

deviation.b) Co-staining of MAP2 (grays), Mitotracker CMXRos and LAMP2 (green) at day 24. c) Confocal images of neurons stained for MAP2 (grays) and with Mitotracker CMXRos (red) at a lower dilution (1:5000, 200nM) to allow detection of mitochondria in processes (day 23). d) Quantification of the Mitotracker entropy and the Mitotracker intensity in the soma (d), as well as the number of mitochondria in axons (e) of day 23 neurons treated with the pLNA-Ctrl or pLNA-1229. Images were acquired from three independent differentiations (72 pictures for the pLNA-Ctrl and 64 pictures for the pLNA-1229 condition). Shown are violin plots of all datapoints together with the mean and standard deviation of each differentiation. A robust linear model was applied over the aggregated means of each condition and differentiation (~ condition + differentiation). Statistical differences were assessed with emmeans. Values were transformed with the square root to account for skewness in the data. f) Example snippet of a video acquired with the structured illumination microscope (SIM) of igNeurons incubated with a mitochondrial dye at day 29. The widefield image is displayed on the left and the processed version on the right. g) Mitochondrial length quantification at two time points (day 29 and day 36) from individual images obtained from the SIM-videos of three independent differentiations (20-23 videos of each condition per time point). Shown are violin plots of all datapoints together with the mean and standard deviation of each differentiation. Values were aggregated per video (mean) and a linear model plus emmeans was used for the statistical analyses (~ condition + differentiation). h) Scheme to illustrate neuronal energy supply by mitochondrial respiration and glycolysis. i) Secreted lactate levels were measured from neuronal media supernatant in a luminescence assay from four independent differentiations. A linear model with emmeans post-hoc analysis was used for the statistics at each time point (~ condition + differentiation). j) Calcium peak intensity (df / F) of human neurons recorded at day 37 from three independent differentiations. GSK-2837808A and AlbuMAX were added to the media from day 16 on to activate mitochondria. Shown are violin plots of all datapoints together with the mean and standard deviation of each differentiation. Statistics were performed on the log-transformed, aggregated values per cell (means) with a linear model accounting for the interaction effect between the pLNA condition and the drug (~ pLNA*drug + differentiation). Post-hoc analysis was done using emmeans (pLNA|drug). pLNAs were generally added to the media for all experiments on day nine. (* = p-value < 0.05, *** = p-value < 0.001, **** = p-value < 0.0001)

Discussion

The prolonged synaptogenesis period in specific areas of the human brain is likely one of the most important determinants of human-specific cognitive and behavioral traits. In this regard, the development of cellular systems (2D, 3D) that mimic human brain development has greatly facilitated the discovery of human-specific aspects of synaptogenesis. Here, we modified a neuronal differentiation protocol allowing us to profile ncRNA expression during the time course of human excitatory synapse development at unprecedented resolution. Thereby, we observed widespread dynamic regulation of several classes of ncRNAs during this period, highlighting the potential importance of the ncRNA regulatory layer in human brain development. By focusing on dynamically expressed, human-specific miRNAs, we identified miR-1229-3p as a potential regulator of the developmental timing of excitatory synaptogenesis. Four point-mutations within the miR-1229 gene, which occurred at the transition from great ape to human, allowed its efficient processing to a mature miRNA. Particularly the nature of miR-1229 being a mirtron and thereby bypassing the regulatory constraints of DROSHA mediated processing might have facilitated this evolutionary adaptation (42). As most of the

recently evolved miRNAs, miR-1229-3p is lowly expressed and therefore likely fine-tunes the expression of many targets within common cellular pathways (43), a notion that fits well with the regulation of mitochondrial homeostasis by miR-1229-3p.

miR-1229-3p slows down excitatory synapse formation, a phenotype that is consistent with a role for miR-1229-3p in human neoteny. Apparently at odds with the synaptotrophic hypothesis, sustained miR-1229-3p inhibition leads to reduced dendritic arborization. However, recent data from cerebellar Purkinje neurons suggests that cumulative synapse formation inhibits further dendrite growth at later stages (44). Thus, we speculate that synaptogenesis induced by miR-1229-3p inhibition triggers a secondary compensatory mechanism to reduce dendritic arborization to maintain neuronal excitability within a physiological range. Mechanistically, we provide molecular and cell biological evidence for the control of mitochondrial homeostasis downstream of miR-1229-3p. In agreement, it has been hypothesized that mitochondria might particularly facilitate synapse formation due to their location at presynapses and energy provision for processes such as local translation (31).

The exact molecular mechanism involved in human synaptogenesis downstream of miR-1229-3p remains to be determined. Among the putative miR-1229-3p targets involved in mitochondrial function, we validated the mitophagy-inducing kinase Pink1. In addition to its role in mitophagy, Pink1 mediated initiation of mitochondrial fission has been directly associated with synapse development (35). However, based on our transcriptomic results, miR-1229-3p dependent regulation of mitochondrial homeostasis likely involves an entire network of genes controlling different aspects of mitochondrial physiology. Recently, it was shown that reduced mitochondrial activity is associated with a delayed maturation of human neurons compared to those of mice (28). Thus, miR-1229-3p dependent inhibition of mitophagy and mitochondrial fission in humans might reflect a lower demand for mitochondrial rejuvenation compared to other species. In the future, it will be important to assess whether inhibition of mitophagy and/or mitochondrial fission is able to revert increased synaptogenesis caused by miR-1229-3p inhibition.

From a clinical point of view, a SNP within the miR-1229 gene, which is expected to increase miR-1229-3p expression, was recently associated with increased risk for Alzheimer's disease (45). Since both mitochondrial fragmentation and mitophagy deficiencies have been implicated in Alzheimer's disease and several other neurodegenerative disorders (38, 46), investigating the role of the miR-1229-3p-Pink1 interaction in such disorders might be a promising direction for future research.

References and Notes:

1. P. Vanderhaeghen, F. Polleux, Developmental mechanisms underlying the evolution of human cortical circuits. *Nat Rev Neurosci* **24**, 213-232 (2023).
2. S. Herculano-Houzel, The remarkable, yet not extraordinary, human brain as a scaled-up primate brain and its associated cost. *Proc Natl Acad Sci U S A* **109 Suppl 1**, 10661-10668 (2012).
3. A. M. M. Sousa, K. A. Meyer, G. Santpere, F. O. Gulden, N. Sestan, Evolution of the Human Nervous System Function, Structure, and Development. *Cell* **170**, 226-247 (2017).
4. C. C. Sherwood, A. Gómez-Robles, Brain Plasticity and Human Evolution. *Annual Review of Anthropology* **46**, 399-419 (2017).
5. W. Enard *et al.*, A humanized version of Foxp2 affects cortico-basal ganglia circuits in mice. *Cell* **137**, 961-971 (2009).
6. C. Charrier *et al.*, Inhibition of SRGAP2 function by its human-specific paralogs induces neoteny during spine maturation. *Cell* **149**, 923-935 (2012).
7. M. Fossati *et al.*, SRGAP2 and Its Human-Specific Paralog Co-Regulate the Development of Excitatory and Inhibitory Synapses. *Neuron* **91**, 356-369 (2016).
8. M. C. King, A. C. Wilson, Evolution at two levels in humans and chimpanzees. *Science* **188**, 107-116 (1975).
9. K. S. Pollard *et al.*, An RNA gene expressed during cortical development evolved rapidly in humans. *Nature* **443**, 167-172 (2006).
10. I. Abugessaisa *et al.*, FANTOM enters 20th year: expansion of transcriptomic atlases and functional annotation of non-coding RNAs. *Nucleic Acids Res* **49**, D892-D898 (2021).
11. K. S. Kosik, T. Nowakowski, Evolution of New miRNAs and Cerebro-Cortical Development. *Annu Rev Neurosci* **41**, 119-137 (2018).
12. G. Zolotarov *et al.*, MicroRNAs are deeply linked to the emergence of the complex octopus brain. *Sci Adv* **8**, eadd9938 (2022).
13. A. M. M. Sousa *et al.*, Molecular and cellular reorganization of neural circuits in the human lineage. *Science* **358**, 1027-1032 (2017).
14. M. Somel *et al.*, MicroRNA-driven developmental remodeling in the brain distinguishes humans from other primates. *PLoS Biol* **9**, e1001214 (2011).
15. T. J. Nowakowski *et al.*, Regulation of cell-type-specific transcriptomes by microRNA networks during human brain development. *Nat Neurosci* **21**, 1784-1792 (2018).
16. H. Y. Hu *et al.*, MicroRNA expression and regulation in human, chimpanzee, and macaque brains. *PLoS Genet* **7**, e1002327 (2011).
17. H. Y. Hu *et al.*, Evolution of the human-specific microRNA miR-941. *Nat Commun* **3**, 1145 (2012).
18. M. Soutschek, G. Schratt, Non-coding RNA in the wiring and remodeling of neural circuits. *Neuron* **111**, 2140-2154 (2023).
19. Y. Zhang *et al.*, Rapid single-step induction of functional neurons from human pluripotent stem cells. *Neuron* **78**, 785-798 (2013).
20. Z. Sun, T. C. Sudhof, A simple Ca(2+)-imaging approach to neural network analyses in cultured neurons. *J Neurosci Methods* **349**, 109041 (2021).
21. E. Berezikov *et al.*, Diversity of microRNAs in human and chimpanzee brain. *Nat Genet* **38**, 1375-1377 (2006).
22. A. Kos *et al.*, MicroRNA-181 promotes synaptogenesis and attenuates axonal outgrowth in cortical neurons. *Cell Mol Life Sci* **73**, 3555-3567 (2016).
23. R. Saba *et al.*, Dopamine-regulated microRNA MiR-181a controls GluA2 surface expression in hippocampal neurons. *Mol Cell Biol* **32**, 619-632 (2012).

24. T. Treiber, N. Treiber, G. Meister, Regulation of microRNA biogenesis and its crosstalk with other cellular pathways. *Nat Rev Mol Cell Biol* **20**, 5-20 (2019).
25. J. C. McCreight, S. E. Schneider, D. B. Wilburn, W. J. Swanson, Evolution of microRNA in primates. *PLoS One* **12**, e0176596 (2017).
26. M. Schornig *et al.*, Comparison of induced neurons reveals slower structural and functional maturation in humans than in apes. *Elife* **10**, (2021).
27. H. Pontzer *et al.*, Metabolic acceleration and the evolution of human brain size and life history. *Nature* **533**, 390-392 (2016).
28. R. Iwata *et al.*, Mitochondria metabolism sets the species-specific tempo of neuronal development. *Science* **379**, eabn4705 (2023).
29. W. Springer, P. J. Kahle, Regulation of PINK1-Parkin-mediated mitophagy. *Autophagy* **7**, 266-278 (2011).
30. M. Soutschek, F. Gross, G. Schratt, P. L. Germain, scanMiR: a biochemically based toolkit for versatile and efficient microRNA target prediction. *Bioinformatics* **38**, 2466-2473 (2022).
31. M. J. Devine, J. T. Kittler, Mitochondria at the neuronal presynapse in health and disease. *Nat Rev Neurosci* **19**, 63-80 (2018).
32. R. Puri, X. T. Cheng, M. Y. Lin, N. Huang, Z. H. Sheng, Mull restraints Parkin-mediated mitophagy in mature neurons by maintaining ER-mitochondrial contacts. *Nat Commun* **10**, 3645 (2019).
33. P. Saftig, W. Beertsen, E. L. Eskelin, LAMP-2: a control step for phagosome and autophagosome maturation. *Autophagy* **4**, 510-512 (2008).
34. A. K. H. Stavoe, E. L. F. Holzbaur, Autophagy in Neurons. *Annu Rev Cell Dev Biol* **35**, 477-500 (2019).
35. Q. Gao *et al.*, PINK1-mediated Drp1(S616) phosphorylation modulates synaptic development and plasticity via promoting mitochondrial fission. *Signal Transduct Target Ther* **7**, 103 (2022).
36. T. Misgeld, T. L. Schwarz, Mitostasis in Neurons: Maintaining Mitochondria in an Extended Cellular Architecture. *Neuron* **96**, 651-666 (2017).
37. N. Ishihara *et al.*, Mitochondrial fission factor Drp1 is essential for embryonic development and synapse formation in mice. *Nat Cell Biol* **11**, 958-966 (2009).
38. C. Doxaki, K. Palikaras, Neuronal Mitophagy: Friend or Foe? *Front Cell Dev Biol* **8**, 611938 (2020).
39. D. Alsina *et al.*, FBXL4 deficiency increases mitochondrial removal by autophagy. *EMBO Mol Med* **12**, e11659 (2020).
40. B. Billups, I. D. Forsythe, Presynaptic mitochondrial calcium sequestration influences transmission at mammalian central synapses. *J Neurosci* **22**, 5840-5847 (2002).
41. S. K. Kwon *et al.*, LKB1 Regulates Mitochondria-Dependent Presynaptic Calcium Clearance and Neurotransmitter Release Properties at Excitatory Synapses along Cortical Axons. *PLoS Biol* **14**, e1002516 (2016).
42. J. O. Westholm, E. C. Lai, Mirtrons: microRNA biogenesis via splicing. *Biochimie* **93**, 1897-1904 (2011).
43. K. Chen, N. Rajewsky, The evolution of gene regulation by transcription factors and microRNAs. *Nat Rev Genet* **8**, 93-103 (2007).
44. Y. H. Takeo *et al.*, GluD2- and Cbln1-mediated competitive interactions shape the dendritic arbors of cerebellar Purkinje cells. *Neuron* **109**, 629-644 e628 (2021).
45. M. Ghanbari *et al.*, Genome-wide identification of microRNA-related variants associated with risk of Alzheimer's disease. *Sci Rep* **6**, 28387 (2016).
46. A. Bera, G. Lavanya, R. Reshma, K. Dev, R. Kumar, Mechanistic and therapeutic role of Drp1 in the pathogenesis of Alzheimer's disease. *Eur J Neurosci* **56**, 5516-5531 (2022).

47. M. Hansen *et al.*, Generation and characterization of human iPSC lines SANi001-A and SANi002-A from mobilized peripheral blood derived megakaryoblasts. *Stem Cell Res* **25**, 42-45 (2017).
48. M. Hansen *et al.*, Generation and characterization of human iPSC line MML-6838-C12 from mobilized peripheral blood derived megakaryoblasts. *Stem Cell Res* **18**, 26-28 (2017).
49. Y. Qi *et al.*, Combined small-molecule inhibition accelerates the derivation of functional cortical neurons from human pluripotent stem cells. *Nat Biotechnol* **35**, 154-163 (2017).
50. R. Nehme *et al.*, Combining NGN2 Programming with Developmental Patterning Generates Human Excitatory Neurons with NMDAR-Mediated Synaptic Transmission. *Cell Rep* **23**, 2509-2523 (2018).
51. S. M. Ho *et al.*, Rapid Ngn2-induction of excitatory neurons from hiPSC-derived neural progenitor cells. *Methods* **101**, 113-124 (2016).
52. M. Lackinger *et al.*, A placental mammal-specific microRNA cluster acts as a natural brake for sociability in mice. *EMBO Rep* **20**, (2019).
53. C. B. Mulholland *et al.*, A modular open platform for systematic functional studies under physiological conditions. *Nucleic Acids Res* **43**, e112 (2015).
54. S. Butkyte *et al.*, Splicing-dependent expression of microRNAs of mirtron origin in human digestive and excretory system cancer cells. *Clin Epigenetics* **8**, 33 (2016).
55. J. M. Baker, F. M. Boyce, High-throughput functional screening using a homemade dual-glow luciferase assay. *J Vis Exp*, (2014).
56. T. Liu *et al.*, Multi-color live-cell STED nanoscopy of mitochondria with a gentle inner membrane stain. *Proc Natl Acad Sci U S A* **119**, e2215799119 (2022).
57. T. J. Nieland *et al.*, High content image analysis identifies novel regulators of synaptogenesis in a high-throughput RNAi screen of primary neurons. *PLoS One* **9**, e91744 (2014).
58. R. Tian *et al.*, CRISPR Interference-Based Platform for Multimodal Genetic Screens in Human iPSC-Derived Neurons. *Neuron* **104**, 239-255 e212 (2019).
59. O. L. Barreto-Chang, R. E. Dolmetsch, Calcium imaging of cortical neurons using Fura-2 AM. *J Vis Exp*, (2009).
60. A. N. Ngo, M. J. Ezoulin, I. Youm, B. B. Youan, Optimal Concentration of 2,2,2-Trichloroacetic Acid for Protein Precipitation Based on Response Surface Methodology. *J Anal Bioanal Tech* **5**, (2014).
61. J. R. Wisniewski, A. Zougman, N. Nagaraj, M. Mann, Universal sample preparation method for proteome analysis. *Nat Methods* **6**, 359-362 (2009).
62. A. Dobin *et al.*, STAR: ultrafast universal RNA-seq aligner. *Bioinformatics* **29**, 15-21 (2013).
63. Y. Liao, G. K. Smyth, W. Shi, featureCounts: an efficient general purpose program for assigning sequence reads to genomic features. *Bioinformatics* **30**, 923-930 (2014).
64. M. D. Robinson, D. J. McCarthy, G. K. Smyth, edgeR: a Bioconductor package for differential expression analysis of digital gene expression data. *Bioinformatics* **26**, 139-140 (2010).
65. R. U. Rahman *et al.*, Oasis 2: improved online analysis of small RNA-seq data. *BMC Bioinformatics* **19**, 54 (2018).
66. D. Risso, J. Ngai, T. P. Speed, S. Dudoit, Normalization of RNA-seq data using factor analysis of control genes or samples. *Nat Biotechnol* **32**, 896-902 (2014).
67. A. J. Whipple *et al.*, Imprinted Maternally Expressed microRNAs Antagonize Paternally Driven Gene Programs in Neurons. *Mol Cell* **78**, 85-95 e88 (2020).

68. R. Patro, G. Duggal, M. I. Love, R. A. Irizarry, C. Kingsford, Salmon provides fast and bias-aware quantification of transcript expression. *Nat Methods* **14**, 417-419 (2017).
69. M. Soutschek, T. Germade, P. L. Germain, G. Schratt, enrichMiR predicts functionally relevant microRNAs based on target collections. *Nucleic Acids Res* **50**, W280-W289 (2022).
70. V. Agarwal, G. W. Bell, J. W. Nam, D. P. Bartel, Predicting effective microRNA target sites in mammalian mRNAs. *Elife* **4**, (2015).
71. S. Rath *et al.*, MitoCarta3.0: an updated mitochondrial proteome now with sub-organelle localization and pathway annotations. *Nucleic Acids Res* **49**, D1541-D1547 (2021).
72. S. Müller-Dott *et al.*, Expanding the coverage of regulons from high-confidence prior knowledge for accurate estimation of transcription factor activities. *bioRxiv*, 2023.2003.2030.534849 (2023).
73. Y. Perez-Riverol *et al.*, The PRIDE database resources in 2022: a hub for mass spectrometry-based proteomics evidences. *Nucleic Acids Res* **50**, D543-D552 (2022).

Acknowledgments: We thank the laboratory of Emile van den Akker for sending us the stem cell lines used in this study. The ribosomal depletion sequencing and proteomics was carried out by the Functional Genomics Center Zurich (FGCZ). Viral vectors were produced by the viral vector facility at the UZH and we particularly thank Jean-Charles Paterna for his advice. Jana Bühler helped establishing the pLNA protocol. Koen Wentinck helped with mitochondrial super resolution imaging in human neurons. We thank Ruilin Tian for sending his Cell Profiler pipeline for dendrite segmentation. FUW-M2rtTA was a gift from Rudolf Jaenisch, pTet-O-Ngn2-puro from Marius Wernig. We are grateful to Emmanuel Sonder for continuous help with the statistics, Cristina Furler for help with cell culture work as well as Silvia Bicker and Roberto Fiore for insightful discussions along the project and proofreading of the manuscript.

Funding: This project was in part funded by a grant from ERA-NET NEURON JTC 2019 (Altered Translation in Autism, “Altruism”; funded by SNF 32NE30_189486) to GS.

Author contributions: MS performed human neuron differentiations, immunohistochemistry, RNA sequencing sample preparation and analysis, protein extraction, synaptogenesis and dendritogenesis analysis, calcium imaging, helped with mitochondrial super resolution imaging, performed mitochondrial morphology and metabolic analyses, statistical analyses and wrote the manuscript. ALB helped with Mitotracker differentiations, staining and analysis as well as mitochondrial super resolution imaging and analysis. SG performed luciferase reporter gene assays. TW performed human neuron differentiations, helped with calcium imaging as well as synaptogenesis and dendritogenesis analysis. DC wrote the script for calcium imaging analysis. FG performed the human microRNA conservation analysis and mRNA-protein correlation analyses in the time course experiment. TG performed circRNA analysis and helped with statistical assessment of time course data. LZ performed label-free proteomics experiments and data analysis. JB supervised the proteomics part of the study. PLG supervised transcriptomic data analysis and advised on the project. JW performed and supervised the electrophysiological recordings. TK performed and supervised the mitochondrial super resolution imaging and advised on the mitochondrial part. GS conceptualized and supervised the project, wrote the manuscript, and coordinated collaborative experiments.

Competing interest: The authors declare no competing interests.

Supplementary Materials:

Materials and Methods

Figs. S1 to S23

Tables S1 to S5